Internal Report
DESY F12-80/01
BONN-IR-80-22
August 1980

FIELD MEASUREMENT AND PARAMETRIZATION OF THE TASSO SOLENOID MAGNET

by

H. M. Fischer and N. Wermes

FIELD MEASUREMENT AND PARAMETRIZATION OF THE TASSO SOLENOID MAGNET

by

H. M. Fischer and N. Wermes

Physikalisches Institut der Universität Bonn

ABSTRACT

Measurements of the main field component taken at regularly spaced points on concentric cylinders were used to parametrize the field inside the TASSO solenoid magnet. The three components are given in terms of Legendre polynomials. In the subvolume which is filled with tracking chambers an accuracy of 0.4 % was achieved by an 8 parameter fit. The entire field volume is reproduced by a 25 parameter fit.

CONTENTS

1. INTRODUCTION

2. THE SOLENOID MAGNET

3. FIELD MEASUREMENTS
   3.1 Coordinate system
   3.2 The field mapping system
   3.3 Measurement program
   3.4 Data inspection and corrections
   3.5 Field results

4. PARAMETRIZATION
   4.1 Method
      4.1.1 Rotational symmetry
      4.1.2 Rotational and midplane symmetry
   4.2 Fitting procedure
   4.3 Fit results
      4.3.1 Numerical values of the fit parameters
      4.3.2 User routines
   4.4 Errors

5. ACKNOWLEDGEMENTS

APPENDIX
REFERENCES
FIGURE CAPTIONS

1. INTRODUCTION

Experiments at storage rings frequently involve large solenoid magnets for momentum analysis of the charged particles emerging from colliding beam interactions. Usually the solenoid axis is aligned along the beam line in a straight section in order to minimize the influence on the circulating beams. The trajectories of the outgoing particles are measured using wire chamber systems inside the field region. The momenta of the individual particles are determined from the curvature of the appropriate tracks. Therefore besides a high spatial accuracy of the wire chambers accurate knowledge of the magnetic field strength along the track is needed.

For the analysis of large numbers of measured events it is of vital interest that the field information is stored in an easily accessible way which does not consume much computer capacity. These requirements are best met by a parametrization of the field map using only a small number of parameters.

This problem has been solved earlier for large bubble chamber magnets. For the 82-inch HBC at SLAC/1/ two components of the magnetic field were measured on a three dimensional rectangular grid. A least square fit to the data was made using a set of polynomials which satisfy Maxwell's equations. There were three motivations for doing such a fit. It served as a check of the consistency of the measured field data and allowed to obtain the third component although only two were measured. The fit finally furnished a reliable description of the field over the entire space of the chamber which could be used in track recognition programs. A similar procedure was reported for the 12-foot bubble chamber at Argonne/2/ and the 2-meter liquid hydrogen bubble chamber/3/ at ITEF-Moscow.

The question which field component to measure and which network of space points to choose was extensively discussed by H. Wind/4/. Using Maxwell's equations he came to the conclusion that all three field components should be measured but only on the boundaries of the region within which the knowledge of the field is required. The field parametrization can then be obtained by fitting these data with harmonic polynomials.

This method was successfully applied for the field parametrization of several H-magnets at CERN where the field had to be known in a region which was essentially a rectangular box.

A quite opposite approach was made recently at KEK/5/ for the field reconstruction of a large aperture spectrometer magnet. After a careful calibration of a three dimensional Hall probe all three output voltages were measured simultaneously at various points inside the volume of interest. The magnetic field components were then determined point by point by an iterative method without the use of magnetic field equations.

The simultaneous measurement of three field components is a difficult task. Small angular misalignments of the probe can cause large errors in the measurements of the minor components. Such contributions induced from the main component can easily be as large as the small component itself. Corrections of this effect are difficult and not very reliable especially for large systems, where the misalignment may change with the position of the probe within the field volume.

Measurements of the main field component are less sensitive to misalignments of the probe. It is however not necessary to measure the two small components if one makes use of the powerful constraints of Maxwell's equations. All field components can then be derived from one scalar potential which satisfies Laplace's equation. As a consequence the knowledge of one component determines the potential and also the other two components.

Using this procedure a Daresbury group/6/ parametrized the Cartesian field components of a large spectrometer magnet in terms of trigonometric and hyperbolic functions. The fit parameters for the field components were determined by fitting the expression for the main field to the measurements.

Here we present a similar work which was done for the solenoid magnet of the TASSO Detector at the DESY e^+e^--storage ring PETRA.

The paper is organized as follows. Section 2 contains a short description of the solenoid magnet. In section 3 we report on the field mapping equipment and on the measurements. A discussion of the parametrization is given in section 4.

Some useful relations for Legendre polynomials are listed in Appendix A. In Appendix B symmetry properties of the magnetic field in a coil are derived.

2. THE SOLENOID MAGNET

The gross features of the magnet are shown in Fig.1. The field is excited by a normal-conducting water cooled coil of 440 cm length and an inner diameter of 273 cm. The conductor consists of an rectangular aluminium bar 2.94×3.64 cm^2 with a central bore of 1.17 cm diameter for cooling. The coil is wound in four layers with a total of 336 windings. The inner surface and some parts of the outer one are covered with a heat shield.

The coil is a self supporting structure. It is suspended to the side yokes by two rods connected with the end flanges on either side. Magnetic flux return is provided by the top and bottom yokes. The maximum excitation current is 5200 A resulting in a maximum field at the center of 0.494 Tesla. The power consumption amounts to 2.8 MW. A summary of the technical data are given in Table 1.

Number of windings	336
Number of layers	4
Number of cooling circuits	56
Conductor width	3.64 cm
Conductor height	2.94 cm
Conductor central bore	1.17 cm
Water pressure	12 bar
Length of coil	440 cm
Inner radius of coil	136.5 cm
Outer radius of coil	146 cm
Maximum current	5200 A
Maximum voltage	$\sim$ 550 V
Power consumption	$\sim$ 2.85 MW
Maximum field strength	0.494 T

Table 1.

The coil was manufactured by BROWN, BOVERIE & CIE (BBC) according to specifications/7/ set by the TASSO groups from the I. Physikalisches Institut der RWTH Aachen, the Physikalisches Institut der Universität Bonn, and the DESY service group B1.

3. FIELD MEASUREMENTS

3.1 Coordinate system

As a reference frame for the measurements we have adopted the coordinate system which is generally used for the TASSO detector (Fig.1). This is defined as follows. The positive z-direction is chosen along the nominal e^+ direction of the storage ring. The y-axis points vertically upwards perpendicular to the beam line. The x-axis is horizontal and points to the center of the storage ring. The origin is chosen to be in the center of the straight section of the PETRA ring.

In the final position the magnet is aligned so that the beam line runs through the center of the circular holes of the side yokes and the side yokes are symmetric with respect to the origin. The coil suspensions are adjusted such that the center line of the coil coincides with the z-axis.

During the field measurements the magnet was positioned outside the beam area at a distance $\Delta x = 6m$. The measuring equipment was aligned to a magnet based system whose axes were parallel to the beam based system with the origin however in the center of the magnet yoke.

The magnet has been designed to provide the main field in the z-direction. Therefore we have large B_z components, small radial components and only a minor azimuthal dependence of the field. Hence it is adequate to the problem to measure and parametrize the components of the magnetic field in a cylindrical system as is shown in Fig.2.

3.2 The field mapping system

The basic requirements which should be met by the field measuring device are the following:

1. It should allow to measure the three components B_z, B_ρ, B_ϕ simultaneously at accurately defined locations everywhere inside the coil volume.

2. After preselection of the step sizes δz, $\delta \rho$, $\delta \phi$ (Fig.3) the device should automatically take readings on a three dimensional cylindrical grid and store the data on tape.

The system we used was designed, built and tested by DESY service group B1. It consisted of the positioning device Messma III, interface electronics and a PDP 8 computer. Programming and maintenance of the PDP 8 was provided by the DESY group F 58.

The field sensing probe consisted of a set of three mutually perpendicular Hall plates embedded in a $10 \times 10 \times 8$ mm^2 cube as shown in Fig.4. The calibration to an accuracy of better than 0.1 % was carried out in a constant homogeneous field using a NMR magnetometer/8/. The positioning of the probe was accomplished by Messma III which is shown in Fig.5.

The basis of Messma III is a lathe-type support (1) which was set up outside the magnet near the beam holes of the side yokes. On this support a carriage (3) could precisely be moved along the z-direction over a total range of Δz = 260 cm. A thick walled aluminium pipe (2) is mounted with one end onto the carriage such that the other end could extend into the field volume. The pipe could be centered along the z-axis by set screws (4) under the main support. A radial arm (5) was connected to the front end of the pipe, whose azimuthal position could be changed from outside by rotation of the pipe.

The Hall probe was mounted on a little carriage which could be pulled forth and back along the radial arm. The movement of the probe carriage, the rotation of the radial arm and the displacement along the z-direction were accomplished remotely by step motors.

The ranges along the three coordinates inside the coil volume were

$$\Delta z = 225 \text{ cm}$$
$$\Delta \rho = 130 \text{ cm}$$
$$\Delta \phi = 360^\circ \quad .$$

The positioning could be done to an accuracy of 0.1 mm in z, 0.2 mm in ρ and 2.5 mrad in ϕ.

The precise alignment of the device was carried out by the survey group of the DESY Hallendienst.

The voltages and the current of the Hall probes, the probe position coordinates and the magnet currents were measured and sequentially displayed by the DVM of the on-line electronics. The readings were immediately written into the memory of the PDP 8 on-line computer and afterwards transferred to DEC tapes. For an easy monitoring of the mapping procedure the last 160 measurements were displayed on the CRT terminal. By means of a multiplexer interface the DEC tape contents could be transferred to the disk of the IBM 370/168 system in the computer center of the Laboratory and therefrom dumped to magnetic tape. A block diagram of the data flow is shown in Fig.6.

3.3 Measurement program

In order to study the behaviour of the magnet we first measured excitation curves at the center of the coil and at some other locations where saturation effects should show up most strongly. The magnetic field as a function of the magnet current turned out to be linear up to the maximum excitation of 5200 A (Fig.7). This result implies that only a field map at maximum excitation is needed for the knowledge of the field at all possible conditions. Nevertheless we made an additional measurement at a medium excitation however with less dense spacings of the measurements. Step sizes and the number of measurements for the two sets are given in Table 3.1.

Magnet current	δz (cm)	$\delta \rho$ (cm)	$\delta \phi$ (°)	No of points
5200 A	10	10	15	18 000
2000 A	15	10	30	5 800

Table 3.1

The determination of a complete field map was complicated by the fact that the z-displacement of the mapping device inside the magnet was limited to a range of 225 cm whereas measurements in the range -220 cm ≤ z ≤ 220 cm were needed.

In order to cover the total coil volume the MESSMA had to be set up on both sides of the magnet to measure the two halves of the field volume seperately. An overlap of the two sets of about 20 cm in the center region gave sufficient information for consistency checks and alignment corrections.

The measuring device could not be aligned such that the grids of the two measurements coincide. Before parametrization of the field within the total coil volume a normalization of the two sets to a common grid was needed. This was accomplished by a spline interpolation.

For an absolute reference during the course of the measurement a NMR probe was positioned on the center line of the magnet at z = ±95 cm. This turned out to be very helpful for the amalgamation of the two data sets.

3.4 Data inspection and corrections

The data on the disk had to be processed before using them as input for the parametrization. The procedure in detail was as follows:

1. Format encoding (PDP 8 to IBM).
2. Conversion of the Hall voltages to magnetic field values.
3. Correction of the field deviations caused by fluctuations of the currents through the hall probe and the magnet.
4. Check of the Hall probe calibration against the readings of the NMR probe taken during the measurements.
5. Three dimensional spline interpolation of the data in order to obtain field values on a grid with equidistant spacings in z, ρ and ϕ.

It turned out that the main corrections were due to the fluctuations of the magnet current; during the measuring period

the power supply was still in a test state in which short time fluctuations as well as long time drifts occured.

3.5 Field results

The general behaviour of the main field component B_z inside the coil volume is illustrated by the three dimensional histogram in Fig. 8. The radial dependence of B_z at various z values is plotted in Fig. 9. Measurements along the x-direction (solid line) and the y-direction (dashed line) are compared to demonstrate the minimal azimuthal dependence which shows up only at large radii. The curves are drawn by eye. Fig. 10 and Fig. 11 show the main field along the center line of the magnet at 5200 A and 2000 A excitation current. The extension of the drift chamber volume is indicated as well.

Further examples of the z-dependence of B_z at larger radii and different ϕ values are given in Fig. 12 and Fig. 13. The radial component B_ρ in the x-z-plane is shown as a function of z in Fig. 14 at ρ = 30 cm and in Fig. 15 at ρ = 100 cm and as a function of ρ at z = 200 cm in Fig. 16.

Frequency distributions of all measured values of the three different field components are plotted in Fig. 17. A summary of the main features of the field and some special values for 5200 A are given in Table 3.2.

B_z at the center	0.493 T
B_z on the axis at z = 170 cm (position of the DC end flange)	0.465 T
B_z on the axis at z = 220 cm (near side yoke)	0.290 T
Radial variation of B_z at z = 0	0.8 %
Radial variation of B_z at z = 170 cm	4.0 %
Max. variation of B_z within DC volume	6.0 %
Azimuthal variation of B_z	0.2 %
Maximum B_ρ	0.1 T
Maximum B_ϕ	0.006 T

Table 3.2

4. PARAMETRIZATION

4.1 Method

In a static magnetic field outside the windings of the coil Maxwell's equations are reduced to

$$\operatorname{div} \vec{B} = 0$$

$$\operatorname{rot} \vec{B} = 0 \quad .$$

Under these conditions the magnetic field $\vec{B}$ can be derived from a scalar potential V

$$\vec{B} = -\operatorname{grad} V$$

which satisfies Laplace's equation

$$\Delta V = 0 \quad .$$

In spherical coordinates (r,θ,ϕ) a solution which is regular at the origin is given by/9/

$$V(r,\theta,\phi) = \sum_{l=0}^{\infty} \sum_{m=0}^{l} (a_{lm} \cos m\phi + b_{lm} \sin m\phi) r^l P_l^m(\cos\theta) \quad (4.1)$$

The associated Legendre polynomials/10/ $P_l^m(\cos\theta) = P_l^m(x)$ form an orthonormal system satisfying the orthogonality relations

$$\int_{-1}^{+1} P_l^m(x) P_{l'}^m(x)\,dx = \frac{2}{2l+1} \frac{(l+m)!}{(l-m)!} \delta_{ll'} \quad . \qquad (4.2)$$

From

$$\vec{B}(r,\theta,\phi) = -\operatorname{grad} V = -\left(\frac{\partial V}{\partial r}, \frac{1}{r}\frac{\partial V}{\partial \theta}, \frac{1}{r \sin\theta} \cdot \frac{\partial V}{\partial \phi}\right)$$

we obtain easily the spherical components of the magnetic field

$$B_r = -\sum_{l=1}^{\infty} \sum_{m=0}^{l} (a_{lm} \cos m\phi + b_{lm} \sin m\phi)\, l r^{l-1} P_l^m(\cos\theta)$$

$$B_\theta = +\sum_{l=1}^{\infty} \sum_{m=0}^{l} (a_{lm} \cos m\phi + b_{lm} \sin m\phi)\, r^{l-1} \sin\theta \frac{d}{d\cos\theta} P_l^m(\cos\theta)$$

$$B_\phi = +\sum_{l=1}^{\infty} \sum_{m=1}^{l} (a_{lm} \sin m\phi - b_{lm} \cos m\phi) \frac{m r^{l-1}}{\sin\theta} P_l^m(\cos\theta) \quad . \quad (4.3)$$

The components of the field in a cylindrical system (z,θ,ϕ) can be calculated from (4.3) by appropriate vector addition through

$$B_z = B_r \cos\theta - B_\theta \sin\theta$$

$$B_\rho = B_r \sin\theta + B_\theta \cos\theta$$

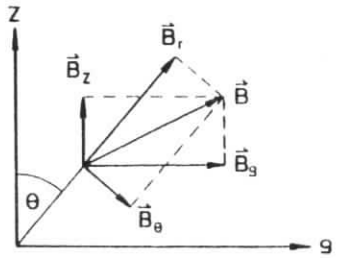

or directly from

$$\vec{B}(z,\rho,\phi) = -\left(\frac{\partial V}{\partial z}, \frac{V}{\partial \rho}, \frac{1}{\rho}\frac{\partial V}{\partial \phi}\right)$$

$$B_z = -\sum_{l=1}^{\infty} \sum_{m=0}^{l} (a_{lm} \cos m\phi + b_{lm} \sin m\phi)\, r^{l-1} (l+m) P_{l-1}^m(\cos\theta)$$

$$B_\rho = +\sum_{l=1}^{\infty} \sum_{m=0}^{l} (a_{lm} \cos m\phi + b_{lm} \sin m\phi) \frac{r^{l-1}}{\sin\theta} [(l+m)\cos\theta P_{l-1}^m(\cos\theta) - l P_l^m(\cos\theta)]$$

$$B_\phi = -\sum_{l=1}^{\infty} \sum_{m}^{l} (a_{lm} \sin m\phi - b_{lm} \cos m\phi) \frac{m r^{l-1}}{\sin\theta} P_l^m(\cos\theta) \quad . \quad (4.4)$$

The potential and the three field components are determined by the same expansion parameters a_{lm} , b_{lm}. Thus a fit to one field component e.g. B_z provides a parametrization of all

three components and the potential as well.

The above relations simplify considerably if the shape of the field meets certain symmetry conditions.

4.1.1 Rotational Symmetry

If the magnetic field shows rotational symmetry (as we expect for an ideal coil) all coefficients a_{lm}, b_{lm} vanish except the $a_{l0} = a_l$. This leads to a potential

$$V(r,\theta) = \sum_{l=0}^{\infty} a_l r^l P_l(\cos\phi) \quad . \tag{4.5}$$

For m = 0 the associated Legendre polynomials are reduced to the "standard" Legendre poynomials (A.4). For the spherical field components we obtain in this case

$$\begin{aligned} B_r &= -\sum_{l=1}^{\infty} l\, a_l r^{l-1} P_l(\cos\theta) \\ B_\theta &= +\sum_{l=1}^{\infty} a_l r^{l-1} \frac{d}{d\cos\theta} P_l(\cos\theta) \\ B_\phi &= 0 \end{aligned} \tag{4.6}$$

and for the cylindrical components by using (A.3) we get

$$\begin{aligned} B_z &= -\sum_{l=0}^{\infty} (l+1) a_{l+1} r^l P_l(\cos\theta) \\ B_\rho &= +\sum_{l=0}^{\infty} a_{l+1} r^l \sin\theta \frac{d}{d\cos\theta} P_l(\cos\theta) \end{aligned} \tag{4.7}$$

4.1.2 Rotational and Midplane symmetry

If the origin of the coordinate system is located in the center of an ideal coil we have symmetry with respect to reflections at the midplane in addition to rotational symmetry.

In this case only odd coefficients a_{2l+1} contribute to the field components (Appendix B)

$$\begin{aligned} B_r &= -\sum_{l=0}^{\infty} (2l+1) a_{2l+1} r^{2l} P_{2l+1}(\cos\theta) \\ B_\theta &= +\sum_{l=0}^{\infty} a_{2l+1} r^{2l} \cdot \frac{d}{d\cos\theta} P_{2l+1}(\cos\theta) \end{aligned} \tag{4.8}$$

While the spherical components contain only terms with odd polynomials the cylindrical components are made up of even ones,

$$\begin{aligned} B_z &= -\sum_{l=0}^{\infty} (2l+1) a_{2l+1} r^{2l} P_{2l}(\cos\theta) \\ B_\rho &= +\sum_{l=0}^{\infty} a_{2l+1} r^{2l} \sin\theta \frac{d}{d\cos\theta} P_{2l}(\cos\theta) \quad . \end{aligned} \tag{4.9}$$

4.2 Fitting procedure

Fitting the field map by a series expansion was motivated by the need of a parametrization which allows to calculate the field fast and accurately enough to be used in track finding programs. This implies that the field components B_z, B_ρ, B_ϕ must be described by a small number of terms. In addition the χ^2 per degree of freedom must be small to ensure a negligible fit error in comparison to measurement uncertainty of 0.0015 Tesla.

To find an optimal solution the fitting of B_z was done successively with the three different assumptions

a) rotational and midplane symmetry
b) rotational symmetry only
c) no symmetry.

For track finding, only the field inside the drift chamber volume must be known. Therefore two different fits were carried out. One covered the field in the range of the drift chamber $-170\ \text{cm} \le z \le 170\ \text{cm}$ and the other was extended over the complete set of measurements within $-220\ \text{cm} \le z \le -220\ \text{cm}$.

4.3 Fit results

The above described procedure showed the following results:

a) If we assume both rotational and midplane symmetry (4.5) we cannot obtain a satisfactory parametrization of the measured data. This is caused by the fact that the field is not symmetric with respect to the origin of the chosen coordinate system.

b) Under the assumption of just rotational symmetry (4.4) the field is already described with high precision. Inside the drift chamber volume a B_z fit with 8 parameters met the requirements almost perfectly. When asking for a description of the total data set however 25 parameters were needed. This increase in the number of coefficients is caused by the stronger inhomogeneities which appear near the side yokes.

c) Using the complete field expressions (4.3) without symmetry restrictions no improvement of the fit was observed. This can be explained by the fact that the azimuthal variation of the field is of the same order (0.2%) as the uncertainties of the measurements.

The deviations of the 8 parameter fit from the measured values of the main field component B_z are plotted in Fig. 18. Using the parameters from this fit to the main field the corresponding B_ρ components were calculated. The deviations of these predictions from the measured B_ρ values are shown in Fig. 19. There is good agreement in the general behaviour of B_ρ. The overall shift of about 0.002 Tesla indicates slight misalignments of the Hall probe which lead to mismeasurements of the small component as already pointed out in chapter 1.

In Fig. 20 and Fig. 21 measurements of B_z are plotted as a function of z and compared with the 8 parameter fit. The radial dependence of B_z at the center and also near the end flange of the drift chamber is shown in Fig. 22 and Fig. 23 together with the fit curves. The prediction of the fit for the radial field B_ρ are compared with a measured radial dependence in

Fig. 24 and with measurements of B_ρ as a function of z in Fig. 25.

Similar comparisons between the 25 parameter fit and the data are shown in Fig. 26 to Fig. 29. Statistical figures of the different fits are listed in Table 4.3. The reader should keep in mind that

- input for the 8 parameter fits are only the data points having $|z| \leq 170$ cm. It is therefore not surprising that deviations for $|z| > 170$ cm occure.
- the figures display only the field B_z in small parts of the total fitted volume. Local disagreements do not prove an overall systematic deviation between fit and measurements.
- in all plots which show the radial component B_ρ the measurements are compared with predictions for B_ρ obtained from the fits to B_z. The existing systematic deviations are due to the inaccuracy of the measurements of the small component B_ρ which has been already discussed in chapter 1.

In the presented procedure only the measured B_z values determine the parametrization of the field. The measurements of the small components were only used for qualitative consistency checks.

	magnet current	fitted volume	no. of deg. of freedom	no. of fit parameter	χ^2/NF
High Field	5200 A	drift chamber $\|z\| \leq 170$ cm	11000	8	0.16
		$\|z\| \leq 220$ cm	15000	25	0.9
Low Field	2000 A	drift chamber $\|z\| \leq 170$ cm	11000	8	0.1
		$\|z\| \leq 220$ cm	15000	25	0.7
assumed data error = 0.0015 Tesla					

Table 4.3

4.3.1 Numerical values of the fit parameters

The coefficients for the fits to the drift chamber subvolume (8 parameters) and to the entire measured volume (25 parameters) are listed in Table 4.3.1. The values are given for the high field and the low field measurements respectively.

The corresponding fit functions

$$B_z = -\sum_{l=0}^{\infty} (l+1) a_{l+1} r^l P_l(\cos\theta)$$

$$B_\rho = +\sum_{l=0}^{\infty} a_{l+1} r^l \sin\theta \frac{d}{d\cos\theta} P_l(\cos\theta)$$

were already discussed in chapter 4.1.1. For practical reasons the radius r has to be inserted in units of 200 cm. The normalization of the Legendre polynomials is given in (4.2).

	LOW FIELD		HIGH FIELD	
	8 PARAMETER FIT	25 PARAMETER FIT	8 PARAMETER FIT	25 PARAMETER FIT
A0	-0.18850E+00	-0.18850E+00	-0.49307E+00	-0.49307E+00
A1	0.21211E-03	0.20186E-03	0.17876E-03	0.95201E-04
A2	-0.79118E-03	-0.88224E-03	-0.21762E-02	-0.24993E-02
A3	0.50125E-02	0.60854E-02	0.12520E-01	0.15286E-01
A4	0.22444E-03	0.40984E-03	0.48626E-03	0.10482E-02
A5	0.17796E-02	0.25914E-02	0.49970E-02	0.68600E-02
A6	-0.21214E-03	-0.81963E-03	-0.46109E-03	-0.19673E-02
A7	-0.50254E-03	-0.22846E-02	-0.14837E-02	-0.51462E-02
A8	0.13349E-03	0.15660E-02	0.25326E-03	0.36104E-02
A9		0.75850E-02		0.20158E-01
A10		-0.30538E-02		-0.56131E-02
A11		-0.22699E-01		-0.65135E-01
A12		0.53341E-02		0.77519E-02
A13		0.49632E-01		0.14396E+00
A14		-0.74492E-02		-0.86107E-02
A15		-0.74926E-01		-0.21889E+00
A16		0.77778E-02		0.73684E-02
A17		0.87543E-01		0.25334E+00
A18		-0.60291E-02		-0.47732E-02
A19		-0.72903E-01		-0.20880E+00
A20		0.33837E-02		0.23913E-02
A21		0.43773E-01		0.12376E+00
A22		-0.12704E-02		-0.85884E-03
A23		-0.16752E-01		-0.46801E-01
A24		0.26397E-03		0.19076E-03
A25		0.37204E-02		0.10210E-01

Table 4.3.1

4.3.2 User routines

Two user routines FLDPAR and FLDMAP have been provided for use in track finding programs.

FLDPAR returns the three field components at a given input space point and magnet current. The CPU-time needed by FLDPAR on the IBM 370/168 computer is about 300 µs for points inside the drift chamber volume and 800 µs for points beyond. A three dimensional interpolation of a stored field map would consume the same amount of CPU-time. So, by the use of FLDPAR the occupation of large arrays for storing a field map can be avoided without any loss of speed.

In addition the routine FLDMAP has been prepared for setting up a map of the solenoid field. The extent and also the step sizes in z, ρ and φ of the grid on which the components of the field are calculated can be individually specified by the user.

4.4 Errors

The measurement error is given by the resolution of the Hall probe system and the alignment uncertainties of the measuring device. Since the second source dominates we determined the total measurement error from the deviation of the Hall probe reading from the reference NMR at the same position. This results in an uncertainty of $\Delta B_z/B_z = 0.3\%$.

The obtained χ^2 per degree of freedom (Tab. 4.3) and the comparison of fit and data in Fig.20-29 show that no additional uncertainty contribution from the parametrization procedure has to be taken into account. Exactly speaking, the quoted error of the measurements may even be overestimated. We nevertheless quote an upper limit of 0.3% since the direct comparison of the NMR reading to the measurement at the same point does account for systematic uncertainties whereas the fit does not.

The measurements of the minor components B_ρ can be strongly modified by slight misalignments of the probe as already mentioned in chapter 1. For this reason B_ρ was calculated from the parametrization of the main field. Therefore we can

assume for B_ρ the same relative uncertainty as for B_z.

The best fit results for the parametrization were obtained under the assumption of rotational symmetry of the field. This implies that $B_\phi = 0$ throughout the entire magnet volume. An indication of the uncertainty of B_ϕ can be obtained from the measured frequency distribution of B_ϕ in Fig. 17. The width of the distribution is mainly caused by the alignment uncertainties. The displacement of the mean value indicates that B_ϕ deviates at maximum 0.002 T from zero.

In summary we can conclude the following total uncertainties

$$\Delta B_z / B_z \leq 0.3\ \%$$

$$\Delta B_\rho / B_\rho \leq 0.3\ \%$$

$$\Delta B_\phi = 0 \pm 0.002 \text{ Tesla} \quad .$$

5. ACKNOWLEDGMENTS

We express our thanks to Dr. Horlitz and the members of the Desy group B1 for the excellent work in building and maintenance of the field mapping system. We are grateful for the help provided by group F58 in programming and maintaining the on-line computer. We wish to thank Dr. Schwickert and the Hallendienst for technical help in preparing the measurements. We are indebted to the service group K for their support during the measuring period. We gratefully acknowledge the helpful conversations with various members of the TASSO collaboration. Finally, we thank our colleagues from the Bonn group for assistance in data taking.

Appendix A

For the sake of the readers convenience we recall some properties of the Legendre polynomials/10/.

Legendre Polynomials $\quad P_n(x) = \frac{1}{2^n\, n!} \frac{d^n}{dx^n} (x^2-1)$

The polynomials of lowest degree are

$P_0(x) = 1$

$P_1(x) = x$

$P_2(x) = \frac{1}{2}(3x^2-1)$

$P_3(x) = \frac{1}{2}(5x^3-3x)$

$P_4(x) = \frac{1}{8}(35x^4-30x^2+3)$

$P_5(x) = \frac{1}{8}(63x^5-70x^3+15x)$

$P_6(x) = \frac{1}{16}(231x^6-315x^4+105x^2-5)$

$P_7(x) = \frac{1}{16}(429x^7-693x^5+315x^3-35x)$

$P_8(x) = \frac{1}{128}(6435x^8-12012x^6+6930x^4-1260x^2+35)$

The $P_n(x)$ obey the relations

$$P_l(-x) = (-1)^l P_l(x) \qquad (A.1)$$

$$P_l'(-x) = (-1)^{l-1} P_l'(x) \qquad (A.2)$$

$$(1-x^2) P'_{l-1}(x) = l(xP_{l-1}(x) - P_l(x)) \qquad (A.3)$$

Associated Legendre Polynomials

$$P_l^m(x) = \sin^m\theta \frac{d^m}{dx^m} P_l(x)$$

In particular we have for $x = \cos\theta$

$P_1^1(x) = (1-x^2)^{\frac{1}{2}} = \sin\theta$

$P_2^1(x) = 3\sin\theta$; $\quad P_2^2(x) = 3\sin^2\theta$

$P_3^1(x) = \frac{3}{2}\sin\theta(5x^2-1)$; $\quad P_3^2 = 15\sin^2\theta$; $\quad P_3^3(x) = 15\sin^3\theta$

For $m = 0$ the $P_l^m(x)$ are reduced to the "standard" Legendre polynomials

$$P_l^0(x) = P_l(x) \; . \qquad (A.4)$$

Appendix B

The following derivations are carried out for the cylindrical components. Similar considerations hold for the spherical case.

If rotational symmetry relativ to the z-axis exists the field components are given by Eq. (4.4).

$$B_z(r,\theta) = -\sum_{l=0}^{\infty} (l+1)\, a_{l+1}\, r^l\, P_l(\cos\theta)$$

$$B_\rho(r,\theta) = +\sum_{l=0}^{\infty} a_{l+1}\, r^l \sin\theta\, \frac{d}{d\cos\theta}\, P_l(\cos\theta)\ .$$

If the origin of the coordinate system is located in the center of an ideal coil and the coil axis coincides with the z-axis then only terms with even l appear in the field parametrization.

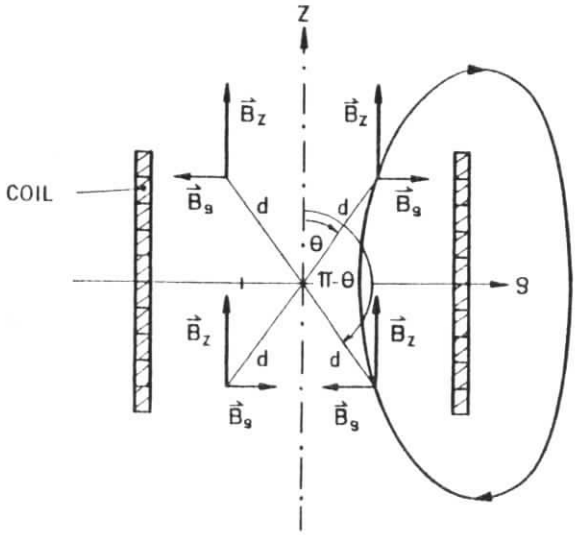

Symmetry relative to the origin requires for the

a) z-component

$$B_z(d,\theta) = B_z(d,\pi-\theta)$$

which implies

$$P_l(x) = P_l(-x)$$

since $(-1)^l P_l(x) = P_l(-x)$

only terms with even l can contribute.

b) ρ-component

$$B_\rho(d,\theta) = -B_\rho(d,\pi-\theta)$$

$$\sin\theta P_l'(x) = -\sin(\pi-\theta) P_l'(-x)$$

since

$$\sin\theta = \sin(\pi-\theta)$$

and

$$(-1)^{l-1} P_l'(x) = P_l'(-x)$$

again follows that only terms with even l survive.

Thus

$$B_z = -\sum_{l=0}^{\infty} (2l+1)\, a_{2l+1}\, r^{2l}\, P_{2l}(\cos\theta)$$

$$B_\rho = +\sum_{l=0}^{\infty} a_{2l+1}\, r^{2l} \sin\theta\, \frac{d}{d\cos\theta}\, P_{2l}(\cos\theta)\ .$$

REFERENCES

(1) S. Flatte and F. Solmitz, Magnetic field of the SLAC 82-inch Hydrogen Bubble Chamber at 4808 amps, SLAC-TN-69-7 (1969).

(2) K. Jaeger, Fits to the three magnetic field measurements of the 12-foot Bubble Chamber, ANL/BBC 153 (1972)

(3) Yu. D. Aleshin, I. L. Kiselevich, V. P. Kulakov, L. I. Kondratev, I. A. Melnichenko, V. I. Mikhailichenko, S. Ya. Nikitin, V. I. Silaev, A.V. Shidlovskii and I. A. Drabkin, Measurement and approximation of the magnetic field of the 2 meter liquid hydrogen bubble chamber at ITEF, Moscow ITEF-87 (1978)

(4) H. Wind, Evaluating a Magnetic Field Component from Boundary Observations Only, Nuclear Instruments and Methods 84 (1970) 117

(5) K. Amako, K. Kawano, T. Matsui and S. Sugimoto, Field Reconstruction for the KEK Large-Aperture-Spectrometer-Magnet "Tokiwa", KEK-78-15

(6) G. F. Pearce, T. J. Brodbeck, G. Frost, G. N. Patrick, D. Newton, A. M. Osborne, T. Sloan, G. R. Brookes, P. B. Wilkes, D. P. Barber, A Method of Field Parametrization for Spectrometer Magnets, Nuclear Instruments and Methods 155 (1978) 371

(7) Spezifikation der TASSO-Spule, DESY, TASSO Internal No. 24 (1977)

(8) K. Knopf, private communication

(9) P. M. Morse and H. Feshbach, Methods of Theoretical Physics, McGraw-Hill Book Company 1953

(10) Jahnke-Emde-Lösch, Tables of Higher Functions, B. G. Teubner Verlagsgesellschaft, Stuttgart 1960

FIGURE CAPTIONS

Fig.1 Schematic view of the TASSO magnet.

Fig.2 Definition of the cylindrical coordinate system.

Fig.3 Space point grid of measurements.

Fig.4 The three component Hall probe system.

Fig.5 Side and front view of the field measuring device.

Fig.6 Block diagram of measuring procedure.

Fig.7 Field excitation curves at different locations.

Fig.8 Histogram of B_z for $\phi = 0°$.

Fig.9 Radial dependence of the axial field B_z for $\phi = 0°$ and $\phi = 90°$.

Fig.10 Main field component B_z along the center line at 5200 A. The size of the drift chamber is indicated.

Fig.11 Main field component B_z along the center line at 2000 A.

Fig.12 z-dependence of B_z at $\rho = 50$ cm and $\phi = 0°$ for 5200 A.

Fig.13 z-dependence of B_z at $\rho = 90$ cm and $\phi = 90°$ at 5200 A.

Fig.14 Radial component B_ρ as a function of z for $\rho = 30$ cm and $\phi = 0°$.

Fig.15 B_ρ as a function of z for $\rho = 100$ cm and $\phi = 0°$.

Fig.16 ρ-dependence of B_ρ for $\phi = 0°$ near the side yoke at $z = 200$ cm.

Fig.17 Frequency distributions of all measured values of the field components B_z , B_ρ and B_ϕ .

Fig.18 Deviations of the 8 parameter fit from the measured B_z values.

Fig.19 Deviations of the predictions for B_ρ of the 8 parameter fit from the measured values.

Fig.20 Comparison of the measured main field component B_z along the center line and the 8 parameter fit (solid line).

Fig.21 z-dependence of the measurements of B_z at $\rho = 50$ cm and $\phi = 90°$ compared with the 8 parameter fit (solid line).

Fig.22 Measured radial dependence of B_z at the center for $\phi = 180°$ compared with the 8 parameter fit (solid line).

Fig.23 Measured radial dependence of B_z at $z = 150$ cm and $\phi = 90°$ compared with the 8 parameter fit (solid line).

Fig.24 Predictions of the 8 parameter fit for the radial field B_ρ (solid line) compared with the measured radial dependence at $z = 150$ cm and $\phi = 270°$.

Fig.25 Predictions of the 8 parameter fit for the radial field B_ρ (solid line) in comparison with measurements as a function of z.

Fig.26 Comparison of the measured main field component B_z along the center line and the 25 parameter fit (solid line).

Fig.27 z-dependence of the measurements of B_z at $\rho = 50$ cm and $\phi = 90°$ compared with the 25 parameter fit (solid line).

Fig.28 Measured radial dependence of B_z at $z = 150$ cm and $\phi = 180°$ compared with the 25 parameter fit (solid line).

Fig.29 Predictions of the 25 parameter fit for the radial field B_ρ (solid line) in comparison with measurements as a function of z.

TASSO - MAGNET

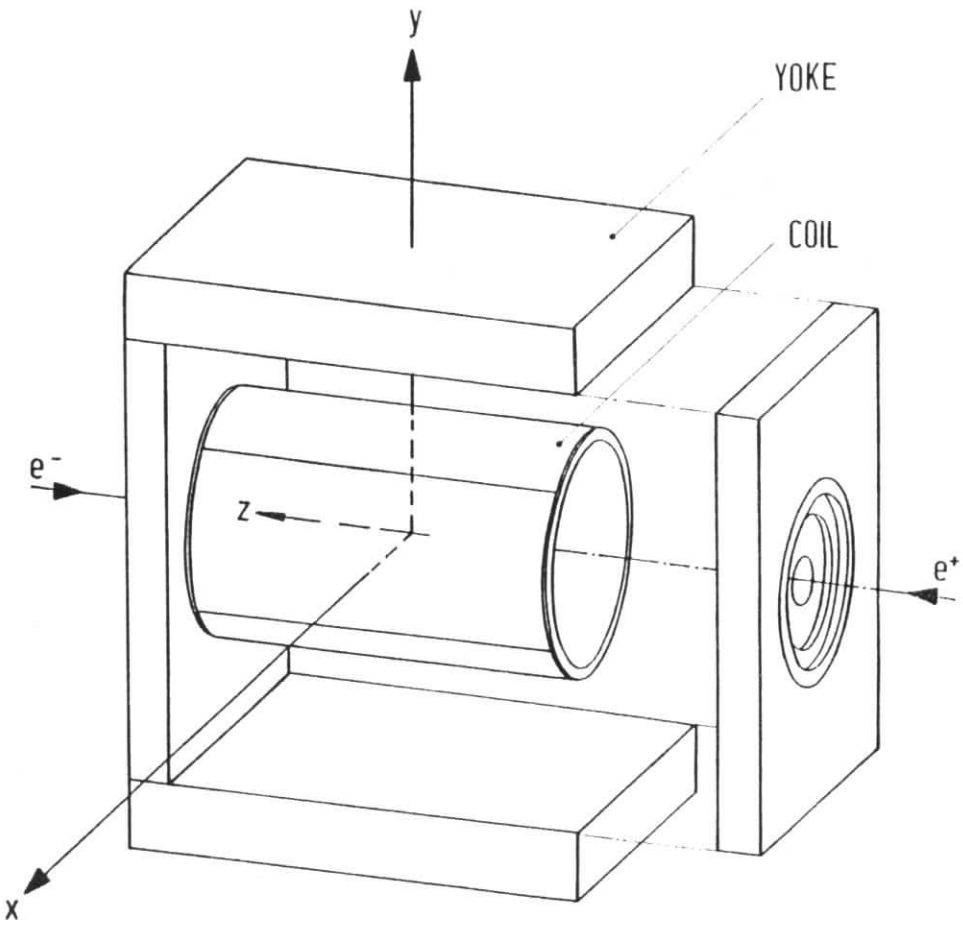

Fig.1

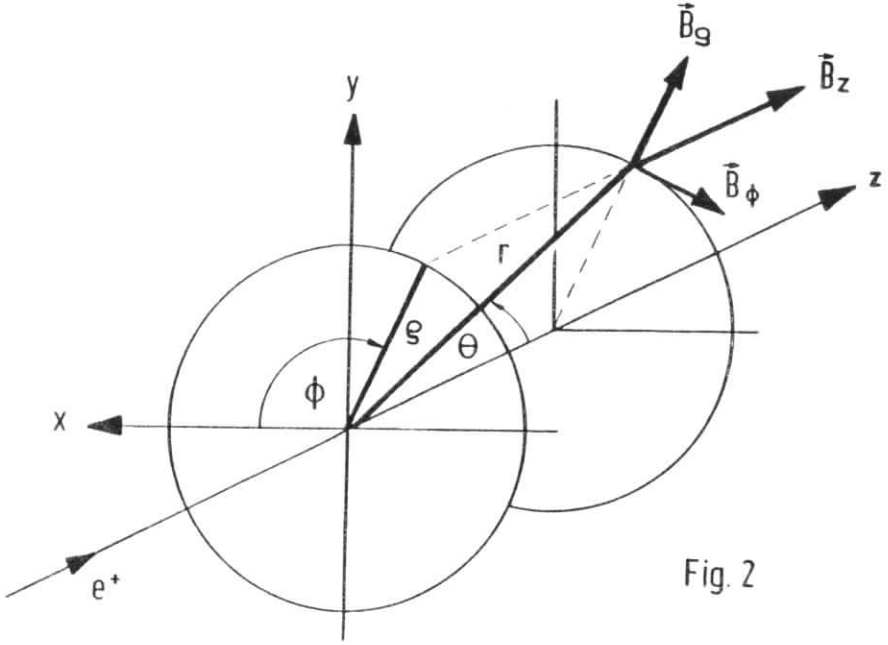

Fig. 2

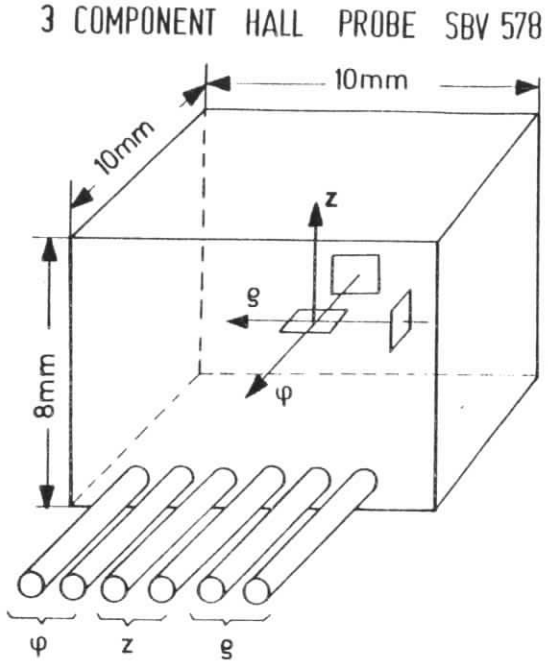

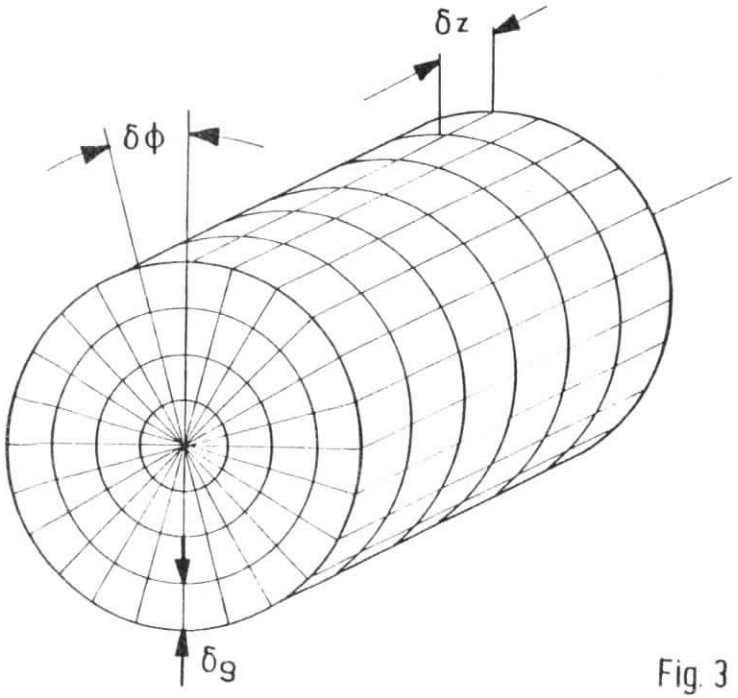

Fig. 3

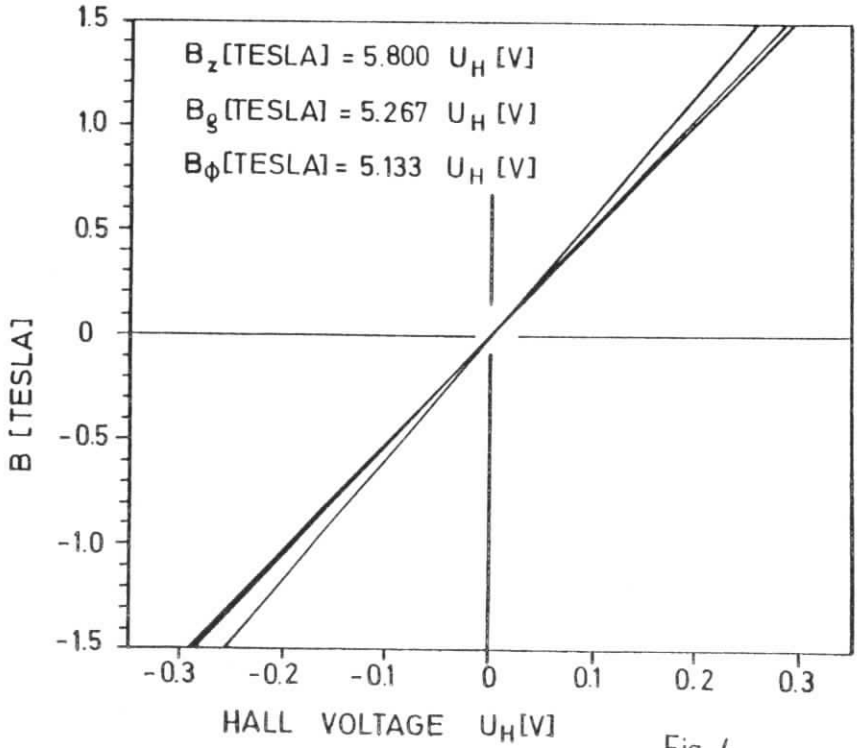

Fig. 4

M E S S M A III

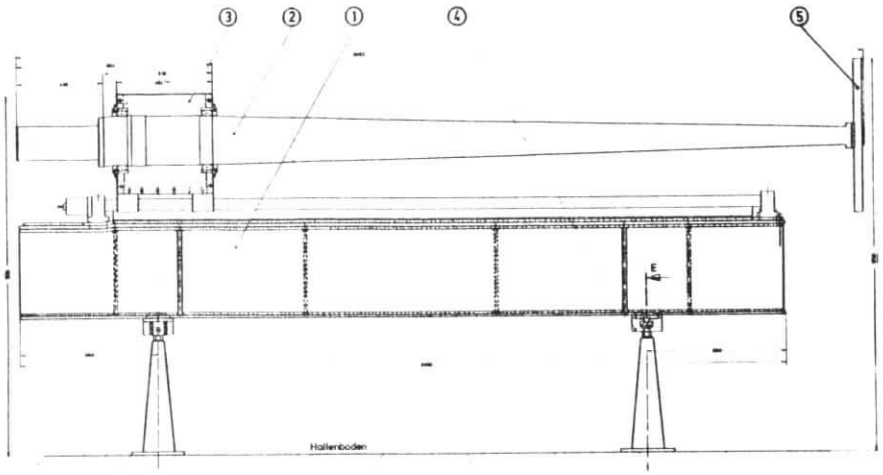

SIDE VIEW

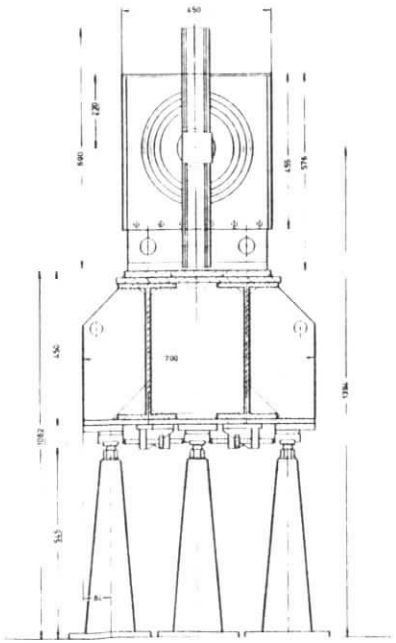

FRONT VIEW

FIG.5

BLOCK DIAGRAM OF DATA FLOW

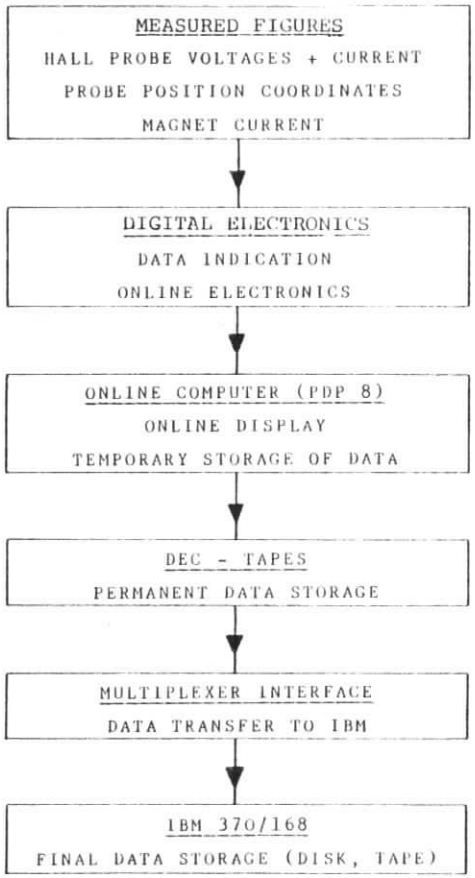

FIG. 6

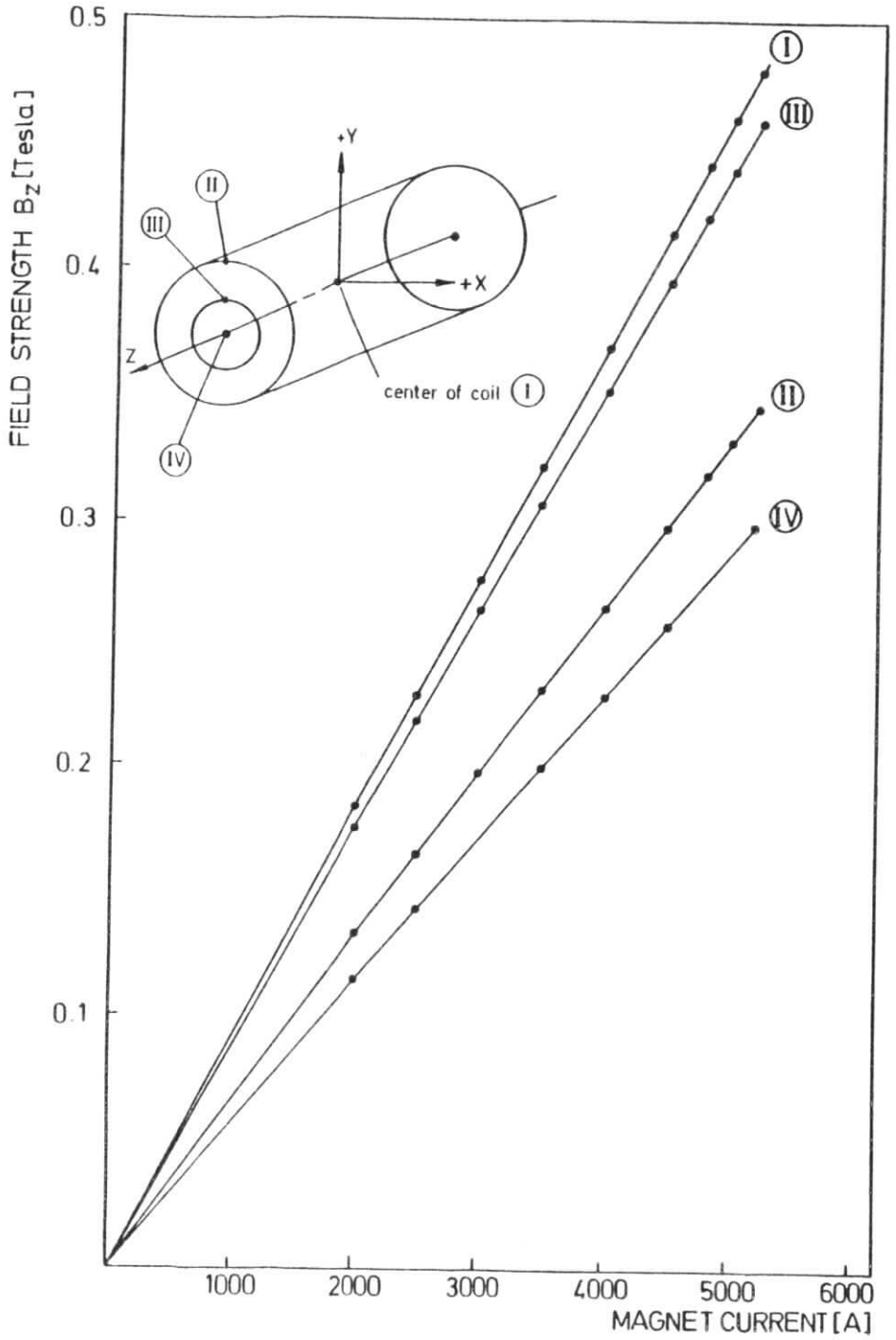
FIELD STRENGTH B_z [Tesla]
0.5
0.4
0.3
0.2
0.1
1000
2000
3000
4000
5000
6000
MAGNET CURRENT [A]
+Y
+X
Z
center of coil (I)
(I)
(II)
(III)
(IV)

Fig. 7

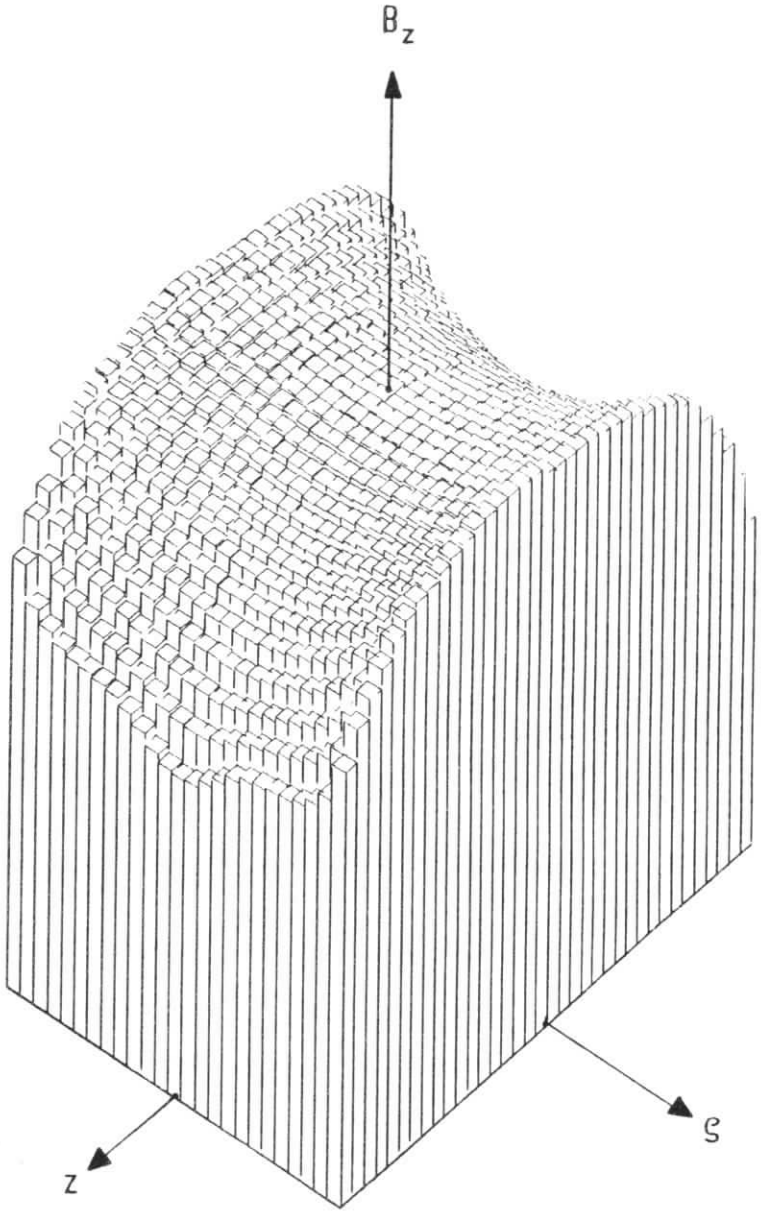
B_z
z
s

Fig. 8

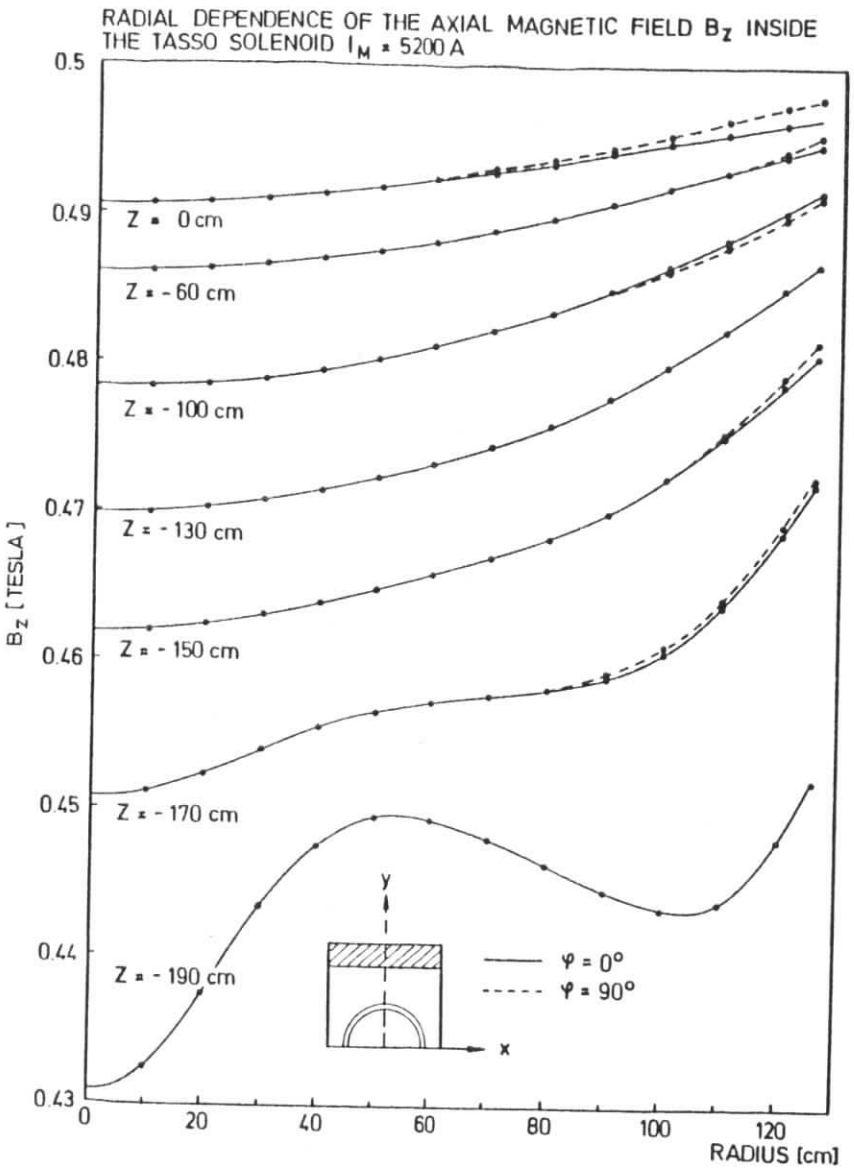

Fig.9

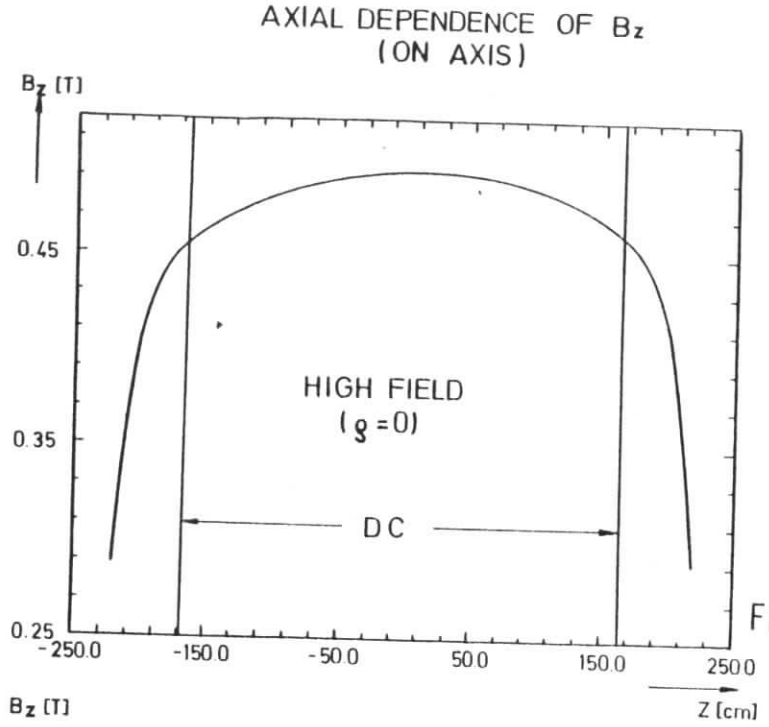

Fig. 10

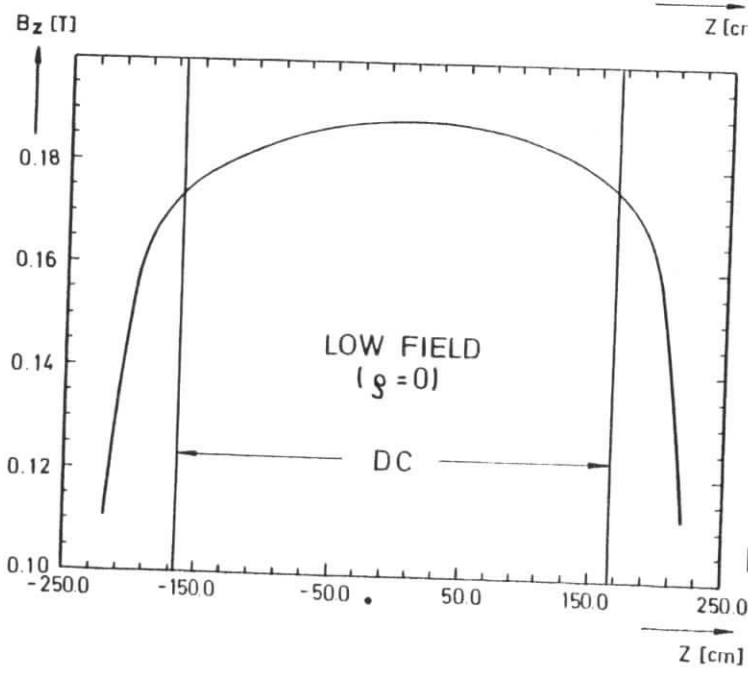

Fig. 11

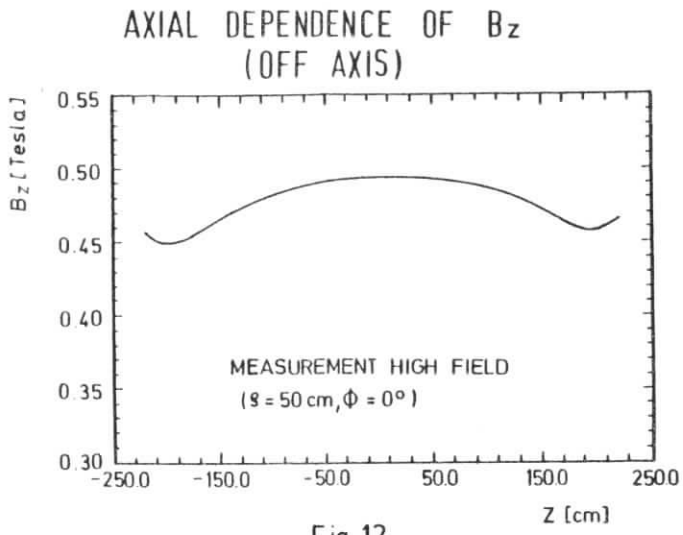

Fig. 12

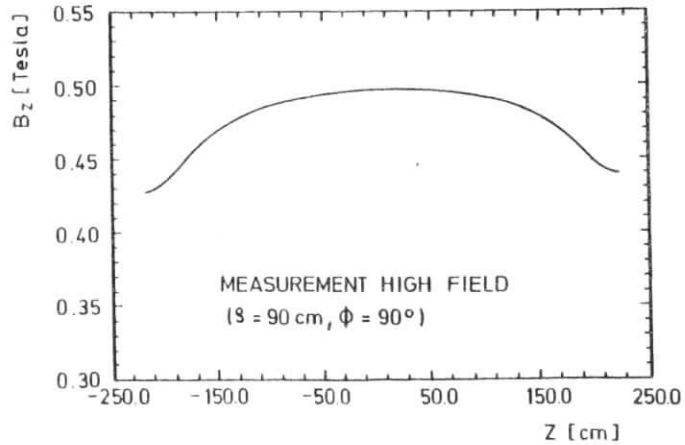

Fig. 13

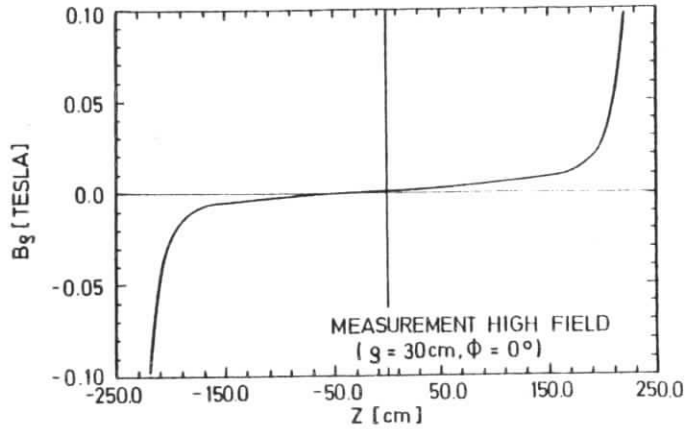

Fig. 14

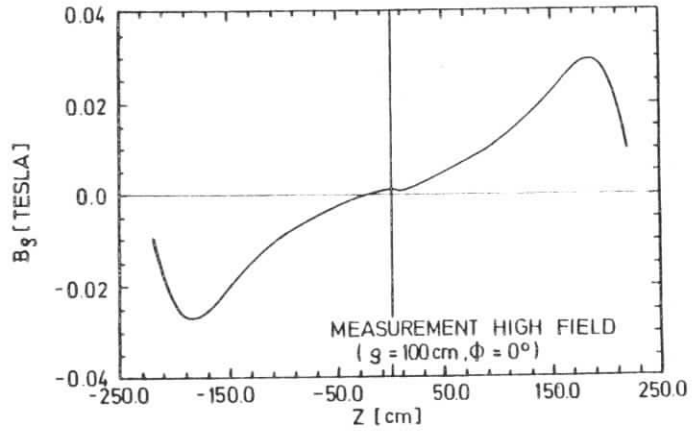

Fig. 15

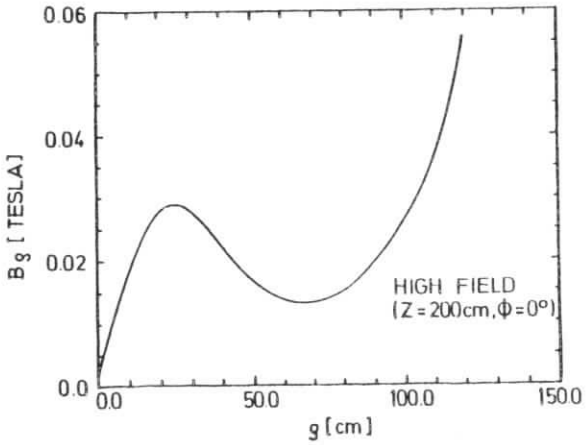

Fig. 16

FREQUENCY DISTRIBUTIONS OF FIELD COMPONENTS

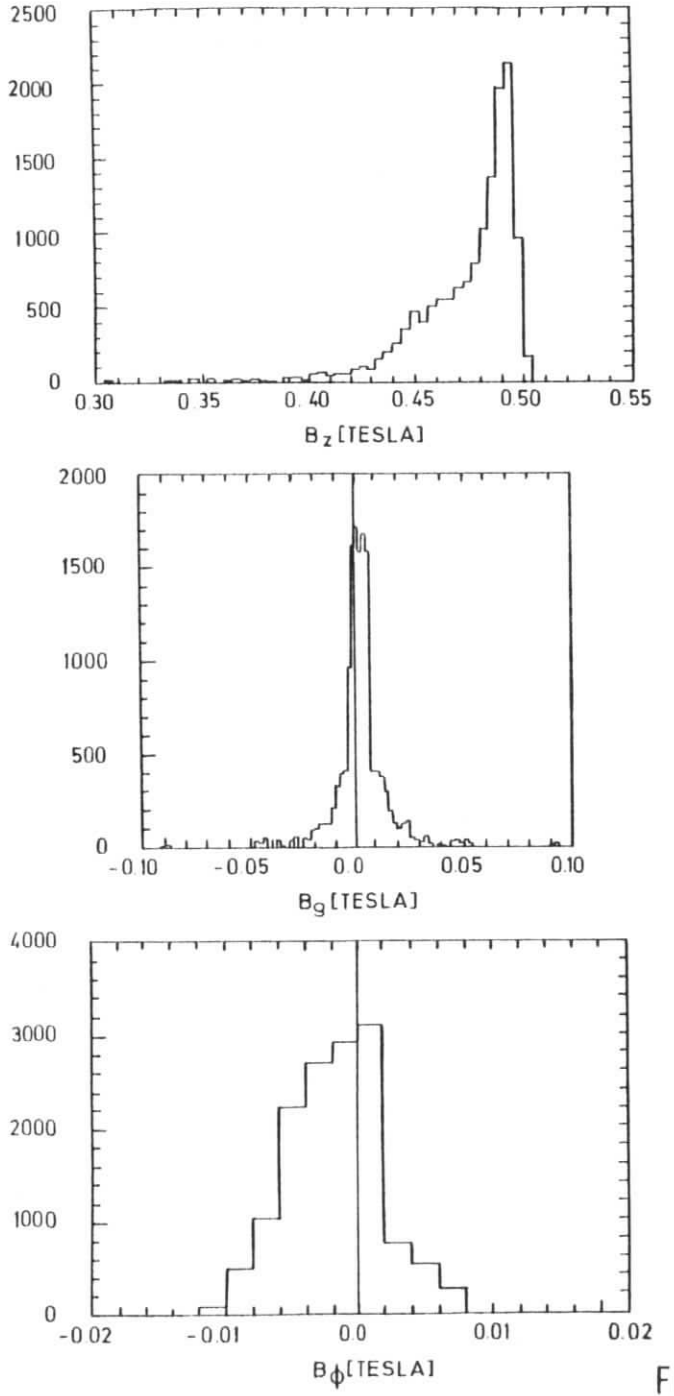

Fig. 17

COMPARISON OF FIT AND MEASUREMENT

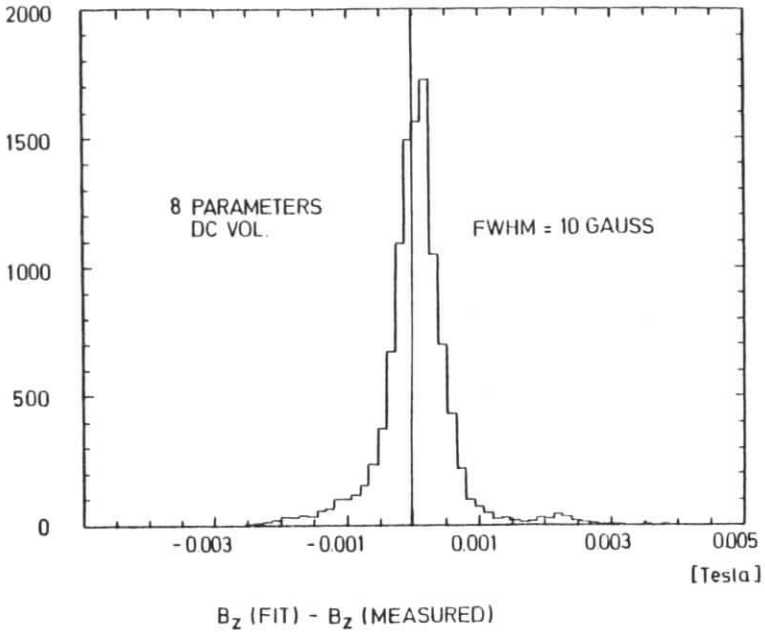

Fig. 18

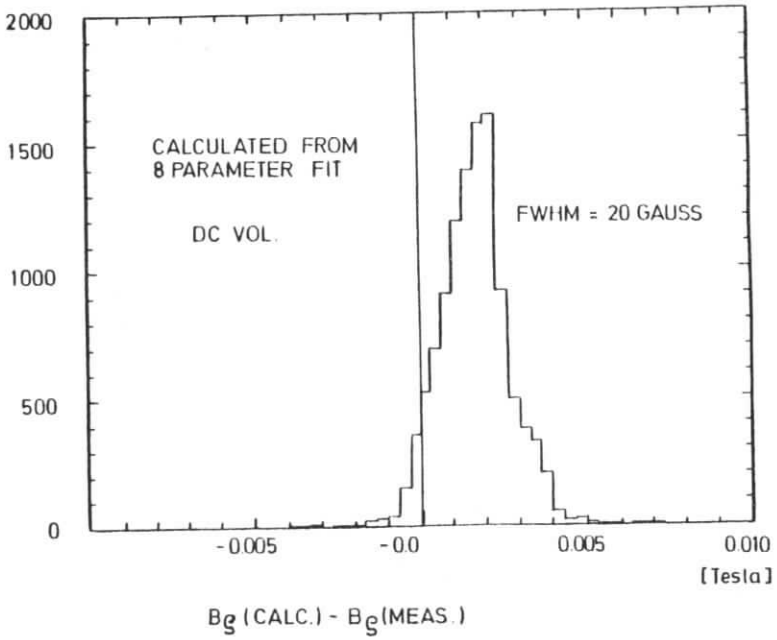

Fig. 19

COMPARISON OF FIT AND MEASUREMENT

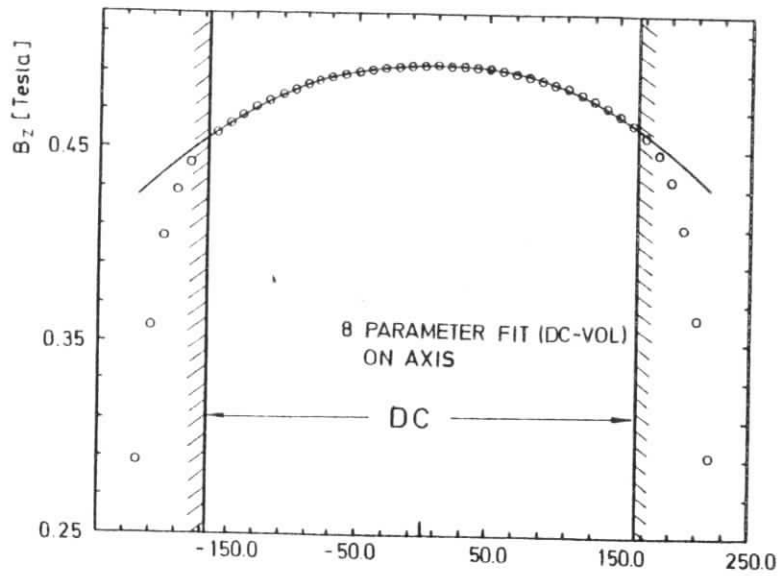

Fig. 20

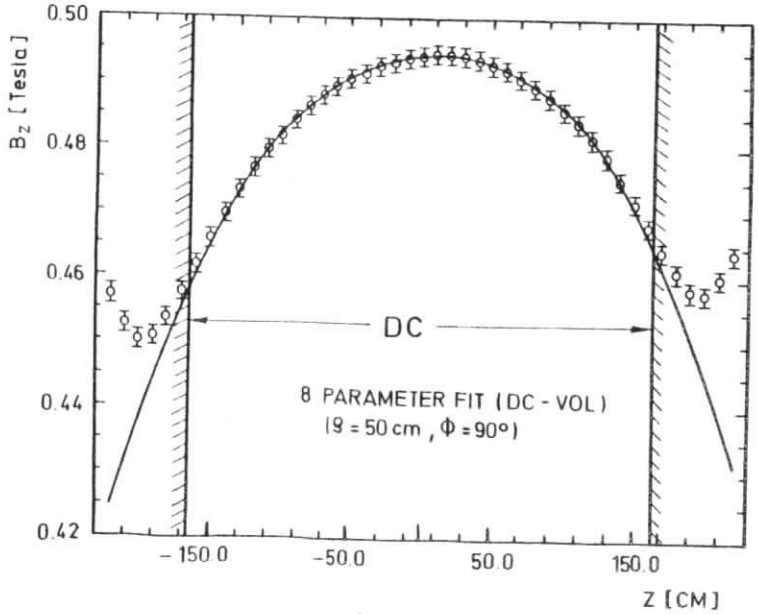

Fig. 21

COMPARISON OF FIT AND MEASUREMENT

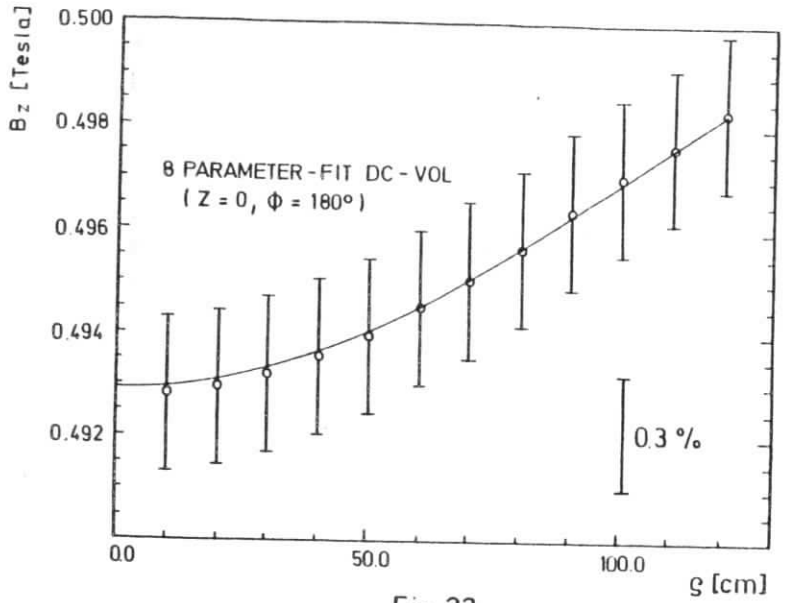

Fig. 22

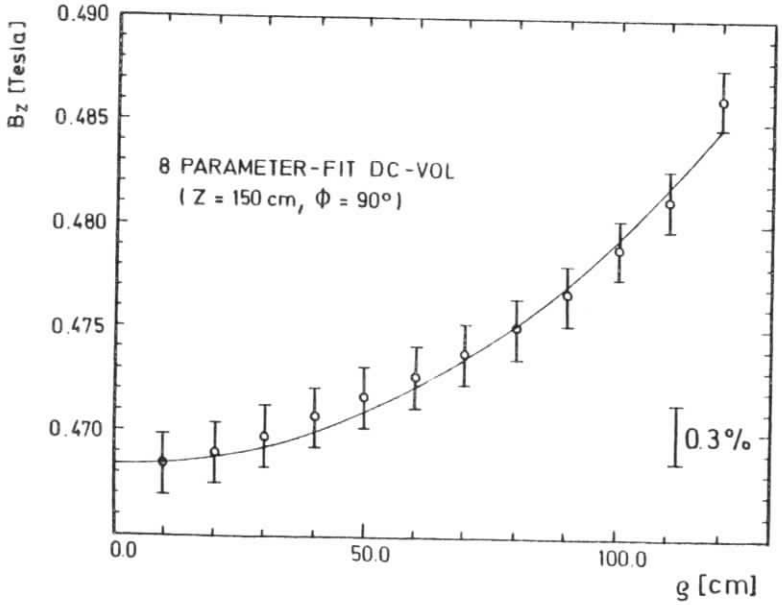

Fig. 23

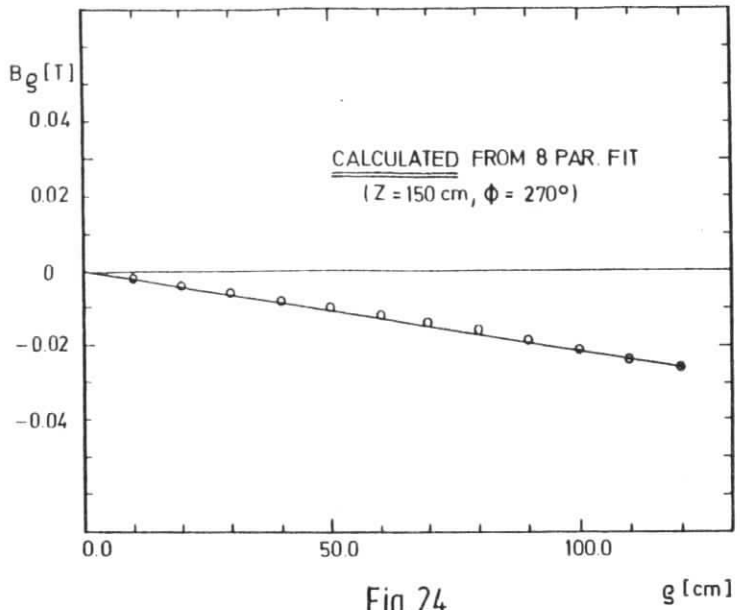

Fig. 24

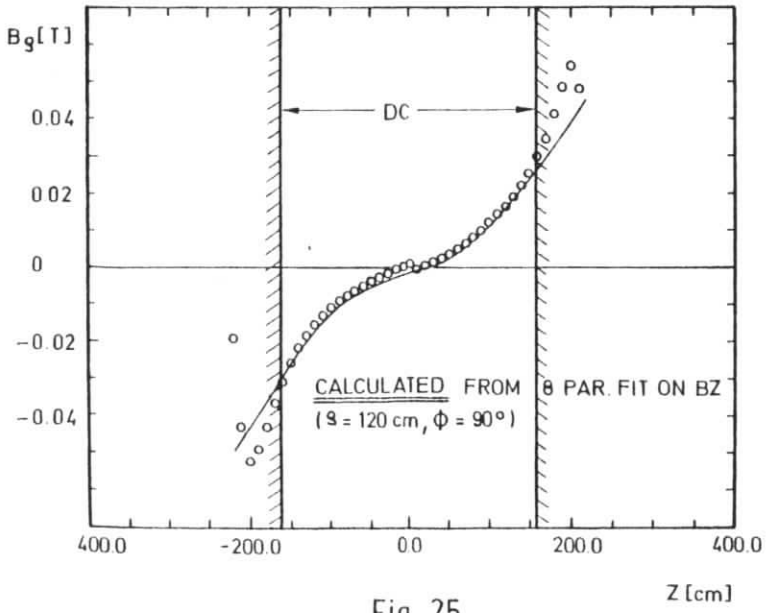

Fig. 25

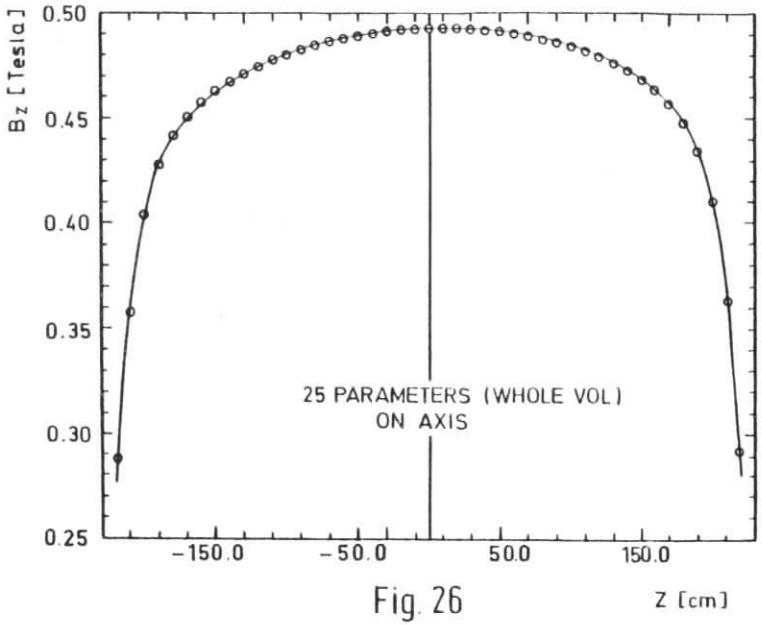

Fig. 26

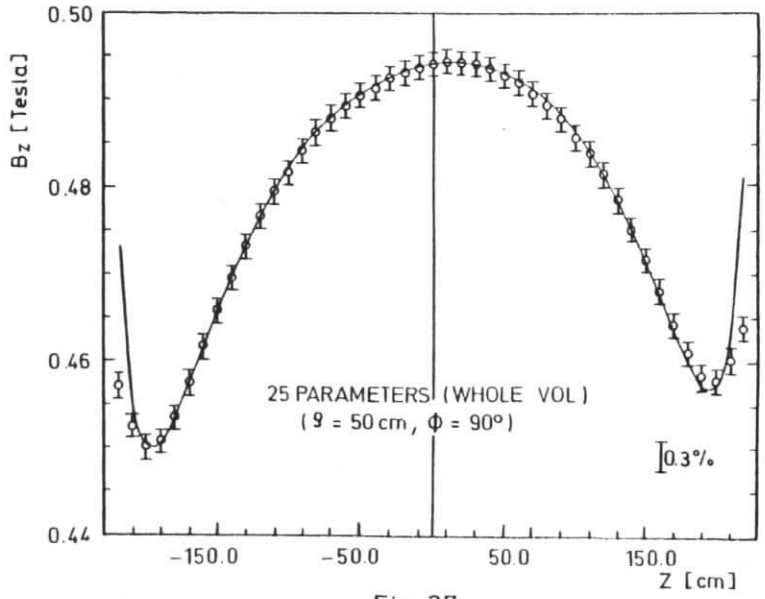

Fig. 27

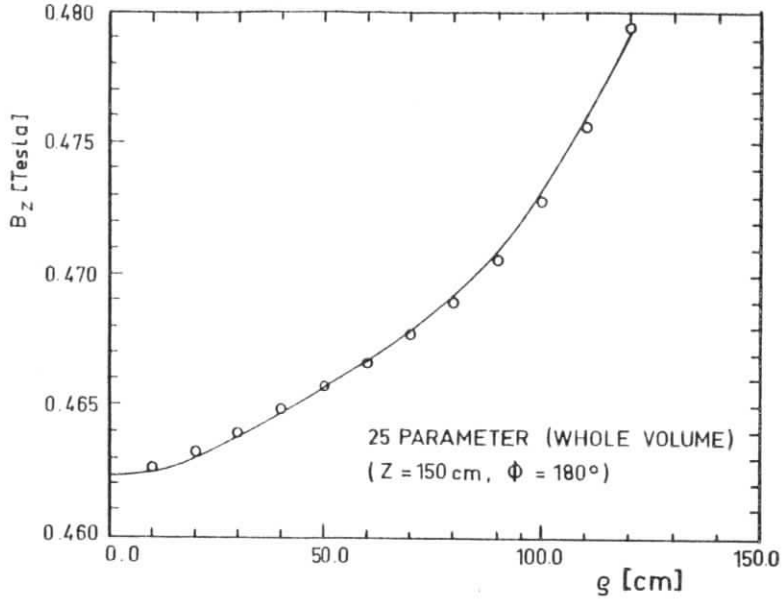
0.480
0.475
0.470
0.465
0.460
B_z [Tesla]
25 PARAMETER (WHOLE VOLUME)
(Z = 150 cm, Φ = 180°)
0.0
50.0
100.0
150.0
ϱ [cm]

Fig. 28

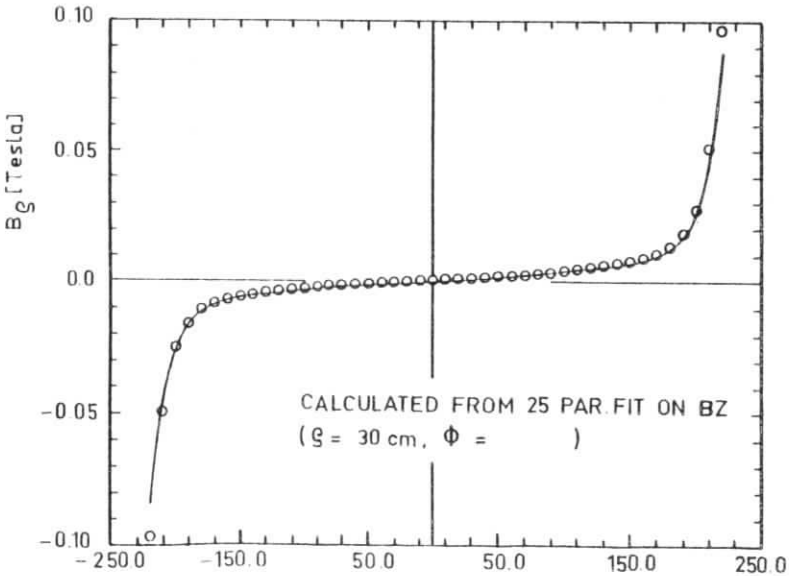
0.10
0.05
0.0
−0.05
−0.10
B_ϱ [Tesla]
CALCULATED FROM 25 PAR. FIT ON BZ
(ϱ = 30 cm, Φ =)
−250.0
−150.0
50.0
50.0
150.0
250.0
z [cm]

Fig. 29